# Controlled Co-operative Wetting Enabled Heterogeneous Structured 3D Morphing Transducers

*Sreepathy Sridhar[1], Cong Wang[1], Jonathan G. Terry[2], Xue Chen[1], Ansu Sun[1], Zhenghong Li[3], Haibao Lv[3], Ben B. Xu[1] and Yifan Li[1]**

Sreepathy Sridhar, Dr. Cong Wang, Dr. Xue Chen, Ansu Sun, Prof. Ben B. Xu, Dr. Yifan Li
Mechanical and Construction Engineering, Faculty of Engineering and Environment, Northumbria University, Newcastle upon Tyne, NE1 8ST, UK
E-mail: yifan.li@northumbria.ac.uk

Dr. Jonathan G. Terry
School of Engineering, University of Edinburgh, Edinburgh, EH9 3JF, UK

Zhenghong Li, Prof. Haibo Lv
Science and Technology on Advanced Composites in Special Environments Laboratory, Harbin Institute of Technology, Harbin, 150080, P.R. CHINA

Keywords:
Heterogeneous hydrogel, droplet microfluidics, responsive swelling, flexible sensors, layer by layer

This paper presents a unique microfluidics approach for functional hydrogel patterning with multi-layered heterogeneous structures. Pre-polymer solution droplets with differentiated sodium acrylate concentrations were dispensed/printed on a wetting-controlled "two-parallel plate" (Hele-Shaw Cell) , where the gelation within the open-microfluidic enable hydrogel bi-layer structures with reconfigurable 3D (3-dimensional) deformations driven by in-plane and through-thickness heterogeneity under stimuli-responsive mask-less swelling/deswelling. The co-operation between swelling-mismatch of functional groups resulted in a higher complexity of 3D reconfiguration in responding to discrete levels of stimulation inputs. This facile-free patterning technology with an in-built ionic hierarchy can be scaled up/down with advanced transducing functionalities in various fields.

## 1. Introduction

Inspired by nature [1-3], morphing soft materials responding to external stimulation (e.g. electrical, mechanical and chemical) have proven to exhibit applicability in various fields [4-9], but not restricted to flexible electronics [10-11], 4D printing [12-13], biomedical transducers [14]

and soft robotics [15-16]. One of the desirable developments is to make the morphing process controllable and programmable through structured soft functional materials, which enables effective shape configuration design according to the applications [4, 16-24]. As one of the popular candidates, hydrogels have drawn more significant attentions due to their open network structures, and ability to generate large changes (therefore high deformation) in volume responding to various external stimulation [16-26]. For example, by creating through-thickness [20], in-plane gradient [27], or combining the two [16, 28] in structuring dissimilar hydrogel functional layers and blocks, controllable deformation such as bending, folding can be achieved.

The through-thickness gradient approach typically employs a hydrogel bi-layer structure, where the swelling behavior remains dissimilar across the thickness [8]. The differential swelling leads to internal stress mismatch and influence out-of-plane 3D morphing configurations, resulting a single configuration at certain external conditions (e.g. temperature, ion concentration) [16]. When external conditions are altered, a wider range of deformation magnitude, and/or a reversed shape (e.g. bending towards opposite direction, "C" becomes "Ↄ") can be achieved, and more complicated configurations can be accomplished via advanced 2D shape patterning [8, 21, 29]. On the other hand, the in-plane gradient approach typically employs 2D heterogeneity via a single layer of patterned functional hydrogel on the same plane, resulting in a bi-stable status where the buckling could happen either directions [16]. Combining the ideas from both through-thickness and in-plane gradient modes, through a controlled "pre-swelling" process that determines swelling direction, programmable complex deformations were demonstrated by the "site-specific" patterned hydrogel blocks [16-17, 27]. The resultant shape morphing structure generated due to in-plane elastic mismatch between non-swelling substrate and controlled swellable gel blocks were more or less fixed [16-17, 27]. Moreover, such approach always requires pairs of silhouetted/holed "pre-swelling masks" to

assist and orchestrate the swelling command, in order to re-configure the deformation patterns [16-17]. Also, once deformed, it will be difficult/impossible to apply the silhouetted/holed mask again to reconfigure the shape. For the required bi-layer system, thickness uniformity is important due to its role in initiating the inherent stress distribution. For homogeneous hydrogel single layer structures, patterned or not, this can be achieved by spin coating, or molding the pre-polymer hydrogel (pre-gel) in a "two-parallel plate" (TPP, like a Hele-Shaw Cell) configuration, followed by gelation processes [8, 30]. Inspired by natural bio-structures, a single layer of encoded heterogeneous hydrogel building blocks has been exploited to form hierarchical complex hydrogel architectures, using droplet microfluidics (DMF) surface wetting control to guide the gel formation [31].

We hereby propose a facile and simple approach to achieve not only programmable, but also reconfigurable mask-less swelling/deswelling morphing structures which change shapes between various co-operative states responding to ionic strength (**Fig. 1**). This reconfigurability was enabled by creating a heterogenous non-functional/functional hydrogel bi-layer, shaped and assembled in a "two-parallel plate" (TPP, like a Hele-Shaw Cell) open-microfluidic configuration during gelation process, based on a setup we firstly revealed during [32]. The structure contains dissimilar high-swelling hydrogel blocks with mismatched swelling behavior, on top of a low-swelling (non-functional) substrate (**Fig. 1a**). The resulted structure will respond to external ionic concentration, with both controllable deformation magnitude and shape reconfiguration (**Fig. 1b**). Such development opens a range of future possibilities, where combining "in-plane" 2D heterogeneity, complex patterns and multi-layer "though-thickness" structures will bring more advanced soft materials morphing control.

## 2. Results and Discussion

### 2.1. Reconfigurable 3D morphing transducers

The hierarchical patterned gels are prepared by two-step polymerization method, as shown in **Fig. 1a**. A thin film non-functional substrate is polymerized to form polyacrylamide (PAAm) gels without the presence of sodium acrylate (SA). PAAm exhibits good biosafety characteristics towards human cells, which makes it a popular candidate in smart bio-medical applications [J. Li et al, Int. J Opthalmol. 2020]. Alongside the non-functional substrate fabrication, a series of patterns made of different concentrations of sodium acrylate containing polyacrylamide mixtures was dispensed onto the pre-coated hydrophilic/hydrophobic template forming the functional blocks. The functional polymer droplets were allowed to crosslink with the pre-fabricated thin-film substrate to achieve multi-patterned 2D hydrogel complex (**Fig. 1b**). The dispersed PAAm gels with various concentrations of sodium acrylate (SA) is shown in table 1. This method provides a no wash "zero-waste", simple step and uniform thickness alternative to conventional fabrication methods such as photopolymerization, extrusion and direct ink writing etc. The multi-state 3D shape reconfiguration mechanism with mask-less swelling/deswelling was then developed and demonstrated (**Fig. 1c**). The number of possible configurations of 3D morphing response to external stimulation can be estimated according to the simple equation given in [16], for combined through-thickness and in-plane gradient modes:

$$2^n \times 1^m = 2^n \qquad (1)$$

where *n* is associated with the number of in-plan gradient units, while *m* is associated with the number of through-thickness gradient units. Applied to our proposed structure in **Fig. 1c**, the bilayer gave *m* = 2, and two dissimilar functional blocks on the same plane gave us *n* = 2, which theoretically leads to 4 possible shape change configurations besides the original state.

### 2.2. Pre-gel droplets wetting control in TPP systems

First, the static CAs of pre-gel droplet on various surfaces were characterized as shown in **Fig. 2a**. these CA values were similar to those of DI (de-ionized) water droplets on the same surfaces. The pre-gel droplet dispensing volume was calculated based on the pattern area (x-y plane in **Fig. 2b**) and the gap distance *g*. When droplet volumes between the two plates were properly dispensed, the CA *θ'* (**Fig. 2c** left) remains between 90° and the advancing CA of the hydrogel on the hydrophilic surface (slightly larger than static CA - 70° for $SiO_2$). When the volume was slightly larger (**Fig. 2c** right), the CA is still acceptable (gel shape still pinned to the wetting pattern), if the *θ'* lies within the pre-gel advancing CAs on hydrophobic surfaces (typically larger than the static CAs of 91°, 109° and 138° for Parylene-C (SCS coatings), FOTS (Perfluorooctyltriethoxysilane, Sigma-Aldrich) and Glaco Zero (Soft 99)) as shown in **Fig. 2a**. Capillary driven flow in a TPP system, where the gap height *g* is significantly smaller than the dimensions of the droplets (**Fig. 2b** and **2c**), the Reynolds number is small enough for us to assume the dynamics can be studied as two-dimensional Hele-Shaw type flow [33], where the capillary pressure equation can be simplified to:

$$P = \kappa_{xy} + \frac{L}{g}\kappa_z \qquad (2)$$

where *L* is the droplet length scale at x-y plane which is significantly larger than *g*.

Later work of open microfluidics [34-35] presented the simplified conditions for the liquid to spread along the hydrophilic area/path when flowing such system, summarized by:

$$\frac{g}{w} < \frac{\cos\alpha + \cos\theta}{2} \qquad (3)$$

where *g* is the gap between top and bottom plates, *w* is the width of the droplet wetting front (functional block pattern dimensions in this work) perpendicular to the direction of flow, $\theta$ and $\alpha$ are the hydrogel static contact angles (CA) on the top and bottom plates respectively (**Fig. 2c**). The droplet will stop spreading when the condition set in equation 2 was not met – e.g. the fluid hits hydrophobic boundary (CA > 90°), and/or the gap *g* is too large (not in our

case as $g << w$). Another special consideration is the pre-gel droplet dispensing volume calculation and control. Once the top and bottom plates are in position ($g$ = spacer thickness), a properly controlled dispensing volume should result in a wetting profile as shown in the left-side of **Fig. 2c**. However, if the dispensing volume is too large, resulting the $\theta' >$ advancing CAs on hydrophobic surfaces, the pre-gel solution will de-pin from the boundary, overflowing the patterns and failing the shape control.

Furthermore, due to the relatively small volume changes during this room temperature crosslinking process, non-functional substrate wrinkling or bending have not been observed during the functional block polymerization in TPP system.

### 2.3. Hydrogel mechanical properties characterization

To understand the deformation behavior of the heterogeneous hydrogel bi-layer structures, mechanical characterization was carried out for functional hydrogel PAAm-SA and the non-functional substrate PAAm. Due to its porous structure, mechanical properties such as the Young's Modulus for hydrogels change during the swelling process [36]. Hence, an in-house developed "clamp-free" tensile testing platform (**Fig. 3a**) was developed to characterize the Young's Modulus of both functional and non-functional hydrogel systemsduring the swelling process. The PAAm composites were casted into the desirable shape using a special mold design which directly integrates with the fixing points of the tensile tester as shown by procedure (i) to (iv) in **Fig. 3a**. **Fig. 3b** shows the strain-stress relationship of the non-functional substrate PAAm thin film (Table 1), immersed in 0.2M and 0.5M PBS solutions for 10 minutes. The Young's Modulus is calculated to be ~10 kPa and ~7 kPa for the PAAm film swelled in 0.2M and 0.5M PBS respectively. And **Fig. 3c** shows the strain-stress relationship of the functional PAAm-SA hydrogel (Pattern I – 1B3S, and Pattern II – 1B1S in Table 1). It can be clearly seen that the higher PBS concentration resulted in higher Young's

Modulus in all cases. We attribute this behavior to highly crystalline nature of the hydrogel molecules reducing the interface defects in the crystalline region and the amorphous area making the elongation longer. The modulus value of the PAAm thin film also matches those reported in [37], which was set as a benchmark.

The swelling and de-swelling ratios dynamically responding to PBS concentration (0 – 0.5M) and SA compositions were obtained. In our previous PAAm-SA (different composition) swelling study [38], various boundary confinement conditions were characterized – free standing, one side confinement, and ring confinement. In this work, the 3D morphing bi-layer structure was placed in "free stand" mode in PBS/water solutions and the swelling ratio characterizations of PAAm and PAAm-SA hydrogel spheres were conducted (**Fig. 4a**). The swelling ratio was given by:

$$Swelling\ ratio = \frac{d_{swell}}{d_{origin}} \qquad (4)$$

**Figure 4b-d** show the swelling ratios of all three PAAm-SA and PAAm compositions (Table 1) over time, in DI water, 0.2M PBS and 0.5M PBS respectively. The PAAm non-functional substrate did not exhibit significant swelling or deswelling behavior, with its diameter topped by 119% of its original value at the end of the tests. For PAAm-SA Pattern I (1B3S in Table 1) and Pattern II (1B1S in Table 1), significant swelling (up to 275%) and deswelling (down to 2%) occurred when immersed in DI water (Fig. 4b) and 0.5M PBS (**Fig. 4d**) respectively. **Fig. 4c** shows the interesting observation that when both PAAm-SA composites were immersed in 0.2M PBS, the Pattern I (1B3S) swells significantly to 241% of its original diameter, while to the opposite Pattern II (1B1S) de-swells significantly to 2% of its original diameter. This large dissimilarity can potentially result in huge deformation magnitudes.

**Due to the high aspect ratio (g<<w, section 2.2) of the TPP molding system, the functional blocks have a large surface area to thickness ratio, compared with the spheres used in swelling test shown in Fig. 4. This has successfully accelerated the reaction time of the transducers with typical an onset of shape morphing occurring around 2 mins of immersion, which was determined by the swelling and deswelling characteristics of the thin functional blocks.**

**2.4. Numerical Modelling of the Reconfigurable Deformation**

Based on the mechanical characterization results obtained, numerical modelling was conducted to help design/programme the morphing configurations under certain external stimulation. Meanwhile the reconfigurability of the same bilayer heterogeneous structure was also studied.

The deformation process of the heterogeneous gel structure is simulated by solving the following mechanical equilibrium equation:

$$\nabla \cdot \underline{\underline{s}} = 0 \qquad (5)$$

where $\underline{\underline{s}}$ is the nominal stress tensor and $\nabla$ is the operator of divergence with respect to the reference state, i.e. the initial state of the gel without swelling or de-swelling. Details of the simulation were included in the *Supporting Information* section.

The in-plane gradient gel structure composed of only two functional blocks can exhibit three different configurations, i.e. straight (non-activated), "S", "C" and "W" shapes as shown in **Fig. 5**. When the functional gel block expands (swells), it will induce an internal tensile stress ($\sigma$) on the top surface of the non-functional substrate, which will generate a clockwise bending moment ($M$) and bend the unit to a convex configuration (**Fig. 5a**). On the other hand, the contracting (de-swelling) gel block induces an internal compressive stress on the top surface of the substrate, which will bend the unit to a concave configuration due to the generated counter-clockwise bending moment (**Fig. 5a**). The radius $R$ of curvature of the unit

depends on the swelling ratio $\rho$ of the gel, and the thicknesses of the gel ($t_g$) and the substrate ($t_s$). Then by scaling analysis, we have:

$$\frac{R}{t_g} = f(\rho, \frac{t_s}{t_g}) \qquad (6)$$

In the simplest case where both the gel block and the substrate are homogeneous and the unit is simplified as Euler-Bernoulli beam, we can further approximate the scaling as:

$$\frac{R}{t_g} = -\frac{t_s/t_g}{2(\rho-1)} \qquad (7)$$

where $R < 0$ corresponds to convex configuration and $R > 0$ corresponds to concave one.

**Fig. 5b** shows the three different cases (reconfigurable states), programmed with two dissimilar functional gel blocks responding to external ion concentration. In the first case where the left gel block (Pattern I) expands (swells) and the right one (Pattern II) contracts (de-swells), the left unit bends to a convex configuration while the right unit bends to a concave one, which lead to an "S" shape of the structure. In the second case, both gel blocks expand, so the two units bend to convex configurations, which make the total structure exhibit a "C" shape. In the third case, both gel blocks contract and the units bend to concave configurations, leading to a "W" shape.

The in-plane gradient gel structure of two different functional blocks is the basic element. By combining more elements, structures exhibiting more complex 3D configurations/shapes can be obtained. **Figure S2a** shows an example of a structure combining three elements which can exhibit a complex 3D wavy configuration.

### 2.5. Re-configurable Multi-state 3D morphing demonstration

The localized swelling and deswelling characteristics of the patterned gels and resulting configurations imparted onto the non-functional substrate are closely related to the ionic

concentration of the environment. The patterned gel's periodicity can be tuned by adding more hydrophilic features onto the hydrophobic Polyacrylic plate. Selective dispensing of functional gels with distinctive sodium acrylate magnitude results in localized spatial configuration that are switchable under different ionic environment (**Fig. 6**). As shown in **Fig. 6a**, both the low (Pattern II) and high concentration (Pattern I) sodium acrylate functional blocks swell in DI water at alternative rate due to ionic-equilibrium and thus forming a concave shape of the non-functional layer. At 0.2M PBS, due to the osmotic imbalance, high concentration sodium acrylate patterned functional block undergoes a positive swelling leading to upward buckling of the non-functional substrate. Whereas, the low concentration sodium acrylate functional block undergoes negative swelling leading to downward buckling resulting in a 'S' shaped configuration (**Fig. 6b**). At 0.5M PBS, due to increase PBS concentration, both the functional groups undergo deswelling forming a 'W' shaped configuration which matches our theoretical simulation results (**Fig. 6c** and **5b**). We believe, the buckling conformation is achieved due to the influence of high transient swelling forces with swelling mismatch occurring in one of the functional blocks [39]. When more than two patterns were involved, complex surface convex and concave buckling can be observed which transients over time with changing diffusion coefficients and ionic equilibrium, as detailed in the *Supporting Information* and Figure S2.

## 3. Conclusion

Reconfigurable multi-state 3D morphing has been achieved through PAAm/PAAm-SA hydrogel bi-layer structure which was created in a "two-parallel plate" (Hele-Shaw Cell) open-microfluidic configuration. The mechanical characterization was carried out to understand the gel property change during the swelling and deswelling processes. The numerical analysis was performed to help understand the morphing states and swelling

configurations, which is in agreement with the experimental observation. The gel structure switching between three different morphing configurations were demonstrated, driven by in-plane and through-thickness heterogeneity during stimuli-responsive swelling subject to ionic concentration change.

Since the PAAm based hydrogel can potentially be engineered to respond to various inputs (e.g. temperature, light, electrical field, magnetic field), we anticipate such heterogeneous multi-layered structures will unlock more advances in the morphing soft transducer applications. For example, a triple-layered (or more) heterogeneous structure exhibiting a dual responsive thermo-electric behaviour can be manufactured to display multiplexed in/output configurations. On the other hand, the re-configurable morphing structure could also be employed for topography induced actuations such as complex topo-optical pattern generation [42]. They can also be attached as a replacement for conventional metallic electrodes, organic electrochemical transistors, with tuneable curvatures to be conformal with complex biological surface topography.Furthermore, the wetting enabled gel assembly and shape-controlled gelation process in TPP systems could potentially be scaled up/down, inspired by existing printing technologies such as ODF (one droplet filling) employed in LCD display manufacturing.

## 4. Experimental Section

*Hydrogel bi-layer preparation*:

The high swelling functional hydrogel pattern I and pattern II were created from poly-acrylamide (PAAm) network with Sodium Acrylate (SA) which contains free positive sodium ions. N,N'-Methylenebisacrylamide (BisAA or MBAA) was used as a cross linker, with N,N,N',N'- Tetramethylethylenediamine (TEMED) and Ammonium Persulfate (APS) used as initiators for the polymerization process.

*Surface treatment of TPP open microfluidics:*

The TPP system consists of a hydrophobically treated Poly-methyl-methacrylate (PMMA) acrylic top plate, and a bottom plate (35 x 80 mm rectangle chip cut from polished silicon wafers) with hydrophobic/philic wetting control patterns. The hydrophilic zone on the bottom plate was 1μm thermally oxidized $SiO_2$ layer. And three different types of hydrophobic coating materials were used: spray coated Glaco Mirro Zero$^{TM}$ (Soft 99), vapour coated Parylene-C (SCS coatings) and FOTS (Perfluorooctyltriethoxysilane, Sigma-Aldrich). The patterning was done via shadow masking (Glaco Zero and FOTS), or photolithography followed by oxygen plasma etching (Parylene-C).

*Hydrogel bi-layer patterning using TPP open microfluidics:*

A detailed recipe of the functional/non-functional substrates is listed in table 1. A 2.5ml of non-functional polyacrylamide solution is dispensed onto the hydrophobic/hydrophilic bottom plate with a defined gap size and gelled to form a thin film (**Fig. 1a**). This was followed by 40μL of polyacrylamide solution with varied sodium acrylate concentration dispensed onto another pre-fabricated hydrophobic/hydrophilic patterned plate with a spacer to adjust the overall thickness of the functional patterns (**Fig. 1a**). For pattern transfer, the PMMA plate containing non-functional thin film is placed over the multi-patterned functional gels and allowed to crosslink. Afterwards, to achieve multi-configurable 3D shape morphing states, the patterned non-functional substrate is allowed to free stand in different ionic concentrations of PBS and water for 10 minutes. The pre-gel solutions were dispensed to polymerize and shaped inside a Hele-Shaw cell (TPP) layered by hydrophobic and hydrophilic boundaries inside the TPP system before polymerization.

**Table 1.** Composition of high-swelling functional hydrogel patterns, and low-swelling non-functional substrate thin film:

| | Acrylamide (wt%) | Bis-Acrylamide (wt%) | TEMED (wt%) | APS (wt%) | **Sodium Acrylate (wt%)** |
|---|---|---|---|---|---|
| **Pattern I (1B3S)** | 18.816 | 3.494 | 0.168 | 1.68 | **16.128** |
| **Pattern II (1B1S)** | 18.816 | 3.494 | 0.168 | 1.69 | **5.376** |
| **Substrate (non-functional thin film)** | 14 | 0.45 | 0.35 | 3.6 | **0** |

*Hydrogel wetting characterization*:

The static contact angle measurement was performed on Kruss DSA30S system. The pre-gel samples were mixed and measured within 15 minutes of preparation. The droplet volumes were kept at 5 μL each, manually dispensed on levelled surfaces with different coatings. The results were presented in **Fig. 2a**.

*Two-parallel-plate (TPP) system setup*:

The construction of the Hele-Shaw Cell system is similar to [40-41], where spacing materials (e.g. plastic shims with thickness range 0.025 – 3 mm) were used as spacers to control the gap height. Firstly, the pre-gel of the non-functional hydrogel substrate – a fine volume controlled low-swelling hydrogel was micro-pipetted within the hydrophilic zone of the bottom plate surface. The PMMA top plate was then lowered towards the bottom plate, leaving a small gap *g* in between. The pre-gel was shaped following the hydrophobic-hydrophilic boundary, with its *thickness* = *g*. The wetting and gelation process observation of the TPP system is explained in the *Supporting Information* document (**Fig. S1**).

**Supporting Information**

Supporting Information is available from the Wiley Online Library or from the author.

**Acknowledgements**

Author 1 and Author 2 contributed equally to this work. This work was supported by EPSRC UK Fluid Network (Grant No. EP/N032861, https://fluids.ac.uk/). The authors would also like to acknowledge other support from the EPSRC (Grant Nos. EP/N007921 and EP/L026899). Data associated with this paper are available via Northumbria Research Data Management scheme.

Received: ((will be filled in by the editorial staff))
Revised: ((will be filled in by the editorial staff))
Published online: ((will be filled in by the editorial staff))

References

[1] S. Armon, E. Efrati, R. Kupferman, E. Sharon, *Science* **2011**, 333, 1726.
[2] I. W. Hamley, V. Castelletto, *Angewandte Chemie International Edition* **2007**, 46, 4442.
[3] S. Li, H. Bai, R. F. Shepherd, H. Zhao, *Angewandte Chemie International Edition* **2019**, 58, 11182.
[4] Y. Liu, J. Genzer, M. D. Dickey, *Progress in Polymer Science* **2016**, 52, 79.
[5] L. Ionov, *Advanced Functional Materials* **2013**, 23, 4555.
[6] X. Liu, J. Liu, S. Lin, X. Zhao, *Materials Today* **2020**, 36, 102.
[7] F. G. Downs, D. J. Lunn, M. J. Booth, J. B. Sauer, W. J. Ramsay, R. G. Klemperer, C. J. Hawker, H. Bayley, *Nature Chemistry* **2020**, 12, 363.
[8] A. Cangialosi, C. Yoon, J. Liu, Q. Huang, J. Guo, T. D. Nguyen, D. H. Gracias, R. Schulman, *Science* **2017**, 357, 1126.
[9] J. Zhao, U. Gulan, T. Horie, N. Ohmura, J. Han, C. Yang, J. Kong, S. Wang, B. B. Xu, *Small* **2019**, 15, 1900019.
[10] K.-I. Jang, K. Li, H. U. Chung, S. Xu, H. N. Jung, Y. Yang, J. W. Kwak, H. H. Jung, J. Song, C. Yang, A. Wang, Z. Liu, J. Y. Lee, B. H. Kim, J.-H. Kim, J. Lee, Y. Yu, B. J. Kim, H. Jang, K. J. Yu, J. Kim, J. W. Lee, J.-W. Jeong, Y. M. Song, Y. Huang, Y. Zhang, J. A. Rogers, *Nature Communications* **2017**, 8, 15894.
[11] H. Fu, K. Nan, W. Bai, W. Huang, K. Bai, L. Lu, C. Zhou, Y. Liu, F. Liu, J. Wang, M. Han, Z. Yan, H. Luan, Y. Zhang, Y. Zhang, J. Zhao, X. Cheng, M. Li, J. W. Lee, Y. Liu, D. Fang, X. Li, Y. Huang, Y. Zhang, J. A. Rogers, *Nature Materials* **2018**, 17, 268.
[12] C. A. Spiegel, M. Hippler, A. Münchinger, M. Bastmeyer, C. Barner-Kowollik, M. Wegener, E. Blasco, *Advanced Functional Materials* **2020**, 30, 1907615.
[13] S. Naficy, R. Gately, R. Gorkin III, H. Xin, G. M. Spinks, *Macromolecular Materials and Engineering* **2017**, 302, 1600212.
[14] A. Kirillova, L. Ionov, *Journal of Materials Chemistry B* **2019**, 7, 1597.
[15] B. J. Cafferty, V. E. Campbell, P. Rothemund, D. J. Preston, A. Ainla, N. Fulleringer, A. C. Diaz, A. E. Fuentes, D. Sameoto, J. A. Lewis, G. M. Whitesides, *Advanced Materials Technologies* **2019**, 4, 1800299.
[16] C. Y. Li, X. P. Hao, S. Y. Zheng, W. Hong, Q. Zheng, Z. L. Wu, *Advanced Intelligent Systems* **2019**, 1, 1900055.
[17] Z. J. Wang, W. Hong, Z. L. Wu, Q. Zheng, *Angew Chem Int Ed Engl* **2017**, 56, 15974.
[18] X. P. Hao, Z. Xu, C. Y. Li, W. Hong, Q. Zheng, Z. L. Wu, *Advanced Materials* **2020**, 32, 2000781.

[19] Z. J. Wang, C. Y. Li, X. Y. Zhao, Z. L. Wu, Q. Zheng, *Journal of Materials Chemistry B* **2019**, 7, 1674.
[20] Y. Zhou, C. M. Duque, C. D. Santangelo, R. C. Hayward, *Advanced Functional Materials* **2019**, 29, 1905273.
[21] C. Y. Li, X. P. Hao, Z. L. Wu, Q. Zheng, *Chemistry – An Asian Journal* **2019**, 14, 94.
[22] X. Zhou, T. Li, J. Wang, F. Chen, D. Zhou, Q. Liu, B. Li, J. Cheng, X. Zhou, B. Zheng, *ACS Appl Mater Interfaces* **2018**, 10, 9077.
[23] S. Y. Zheng, Y. Shen, F. Zhu, J. Yin, J. Qian, J. Fu, Z. L. Wu, Q. Zheng, *Advanced Functional Materials* **2018**, 28.
[24] G. Gao, Z. Wang, D. Xu, L. Wang, T. Xu, H. Zhang, J. Chen, J. Fu, *ACS Appl Mater Interfaces* **2018**, 10, 41724.
[25] B. Xu, R. C. Hayward, *Advanced Materials* **2013**, 25, 5555.
[26] B. B. Xu, Q. Liu, Z. Suo, R. C. Hayward, *Advanced Functional Materials* **2016**, 26, 3218.
[27] Z. J. Wang, C. N. Zhu, W. Hong, Z. L. Wu, Q. Zheng, *Science Advances* **2017**, 3, e1700348.
[28] R. M. Erb, J. S. Sander, R. Grisch, A. R. Studart, *Nature Communications* **2013**, 4, 1712.
[29] Y. Zhang, X. Le, Y. Jian, W. Lu, J. Zhang, T. Chen, *Advanced Functional Materials* **2019**, 29, 1905514.
[30] S. Park, D. Kim, S. Y. Ko, J.-O. Park, S. Akella, B. Xu, Y. Zhang, S. Fraden, *Lab on a Chip* **2014**, 14, 1551.
[31] M.-Y. Chiang, Y.-W. Hsu, H.-Y. Hsieh, S.-Y. Chen, S.-K. Fan, *Science Advances* **2016**, 2, e1600964.
[32] C. Wang, S. Sridhar, J. G. Terry, A. Sun, Z. Li, H. Lv, B. B. Xu, Y. Li, presented at 2019 20th International Conference on Solid-State Sensors, Actuators and Microsystems & Eurosensors XXXIII (TRANSDUCERS & EUROSENSORS XXXIII), 23-27 June 2019, **2019**.
[33] S. W. Walker, B. Shapiro, *Journal of Microelectromechanical Systems* **2006**, 15, 986.
[34] U. N. Lee, J. H. Day, A. J. Haack, R. C. Bretherton, W. Lu, C. A. DeForest, A. B. Theberge, E. Berthier, *Lab on a Chip* **2020**, 20, 525.
[35] B. P. Casavant, E. Berthier, A. B. Theberge, J. Berthier, S. I. Montanez-Sauri, L. L. Bischel, K. Brakke, C. J. Hedman, W. Bushman, N. P. Keller, D. J. Beebe, *Proceedings of the National Academy of Sciences* **2013**, 110, 10111.
[36] J. Macron, A. P. Gerratt, S. P. Lacour, *Advanced Materials Technologies* **2019**, 4, 1900331.
[37] A. K. Denisin, B. L. Pruitt, *ACS Applied Materials & Interfaces* **2016**, 8, 21893.
[38] Y. Li, D. Wang, J. Richardson, B. B. Xu, *Macromolecular Symposia* **2017**, 372, 127.
[39] A. Ilseng, V. Prot, B. H. Skallerud, B. T. Stokke, *Journal of the Mechanics and Physics of Solids* **2019**, 128, 219.
[40] I. Schmueser, E. O. Blair, Z. Isiksacan, Y. Li, D. K. Corrigan, A. A. Stokes, J. G. Terry, A. R. Mount, A. J. Walton, presented at 2020 IEEE 33rd International Conference on Microelectronic Test Structures (ICMTS), 4-18 May 2020, **2020**.
[41] Y. Li, E. O. McKenna, W. Parkes, A. R. Pitt, A. J. Walton, *Applied Physics Letters* **2011**, 99.
[42] C. Wang, D. Wang, V. Kozhevnikov, X. Dai, G. Turnbull, X. Chen, J. Kong, B. Z. Tang, Y. Li, B. B. Xu, *Nat. Commun.* **2020**, 11, 1448

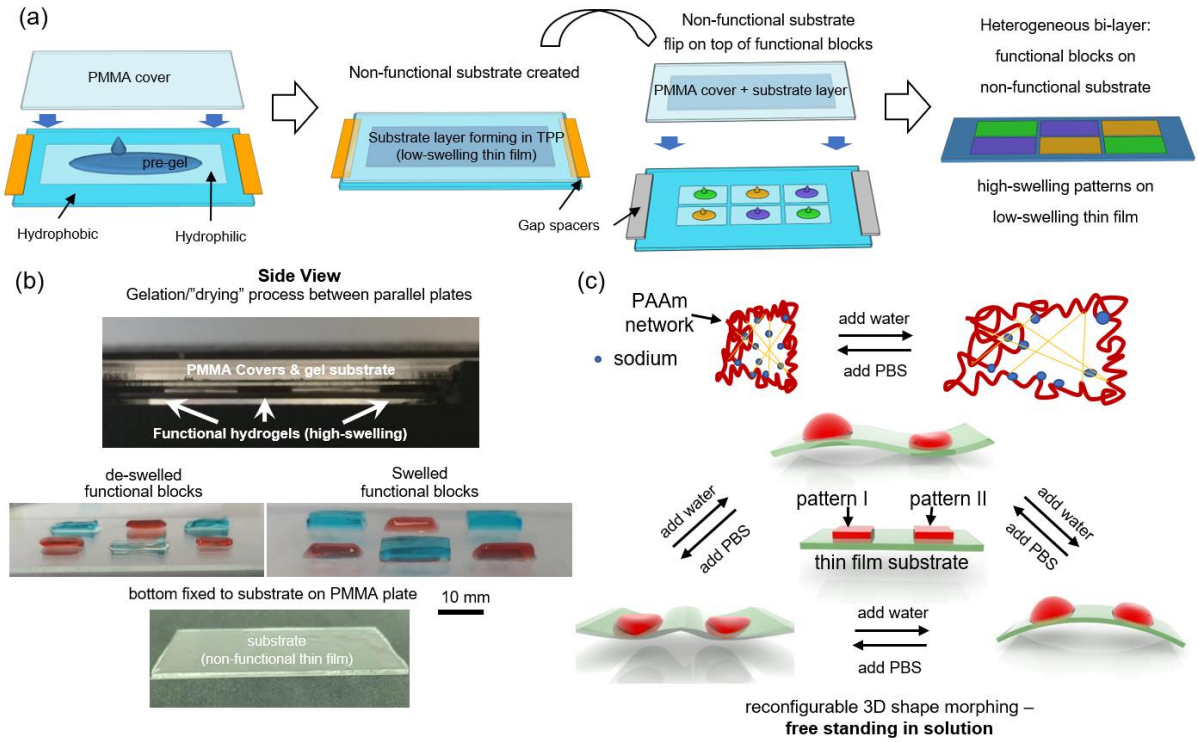


**Figure 1.** Concept of the heterogeneous structured 3D morphing transducers: (a) Bi-layer hydrogel heterogeneous structure fabrication process, using droplet/open microfluidics in a TPP system with wetting control; (b) Experimental photos showing the side view of the gelation process in TPP, with dissimilar swelling behavior demonstrated on substrate fixed to a PMMA plate. (c) Concept demonstration: multi-state 3D shape reconfiguration guided by ionic environment using mask-less swelling/deswelling mechanism, (yellow lines in PAAm network represents crosslinker).

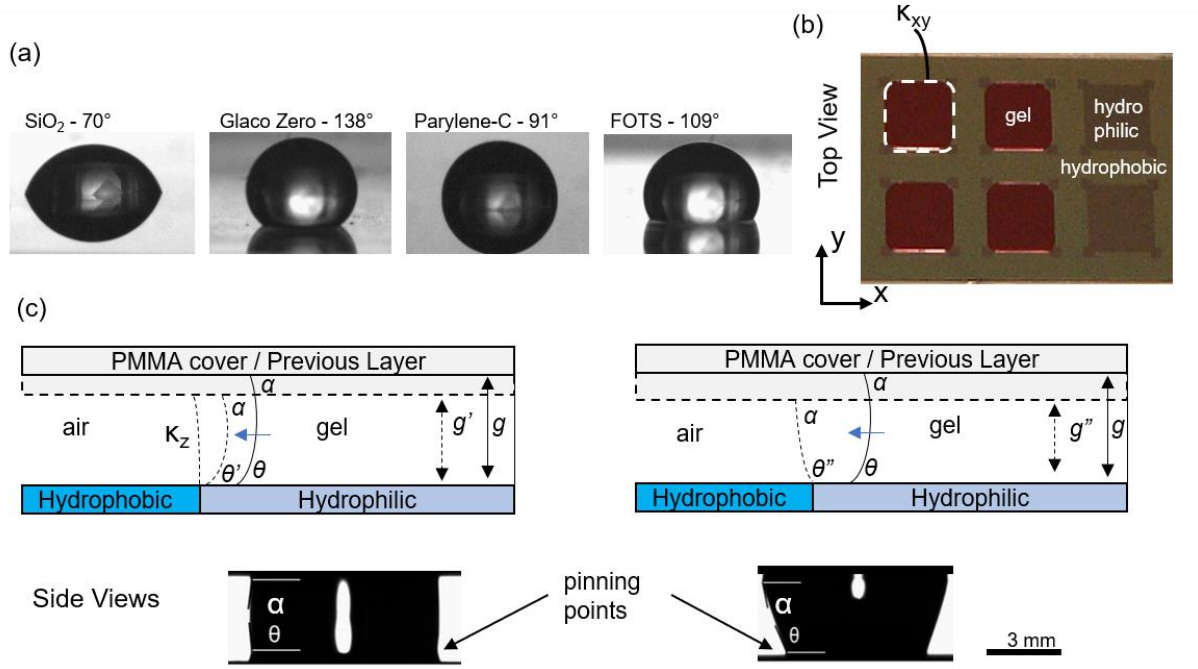


**Figure 2.** The wetting behaviour of the pre-gel PAAm-SA droplets: (a) Static contact angle (CA) measurements by DSA; (b) top view experiment photo of the TPP system with pre-gel

droplets (red color dyed) assembled and shaped by wetting boundaries; (c) side view schematic and experiment photo of the TPP system showing pre-gel droplets spread on hydrophilic patterns and were pinned to the boundaries.

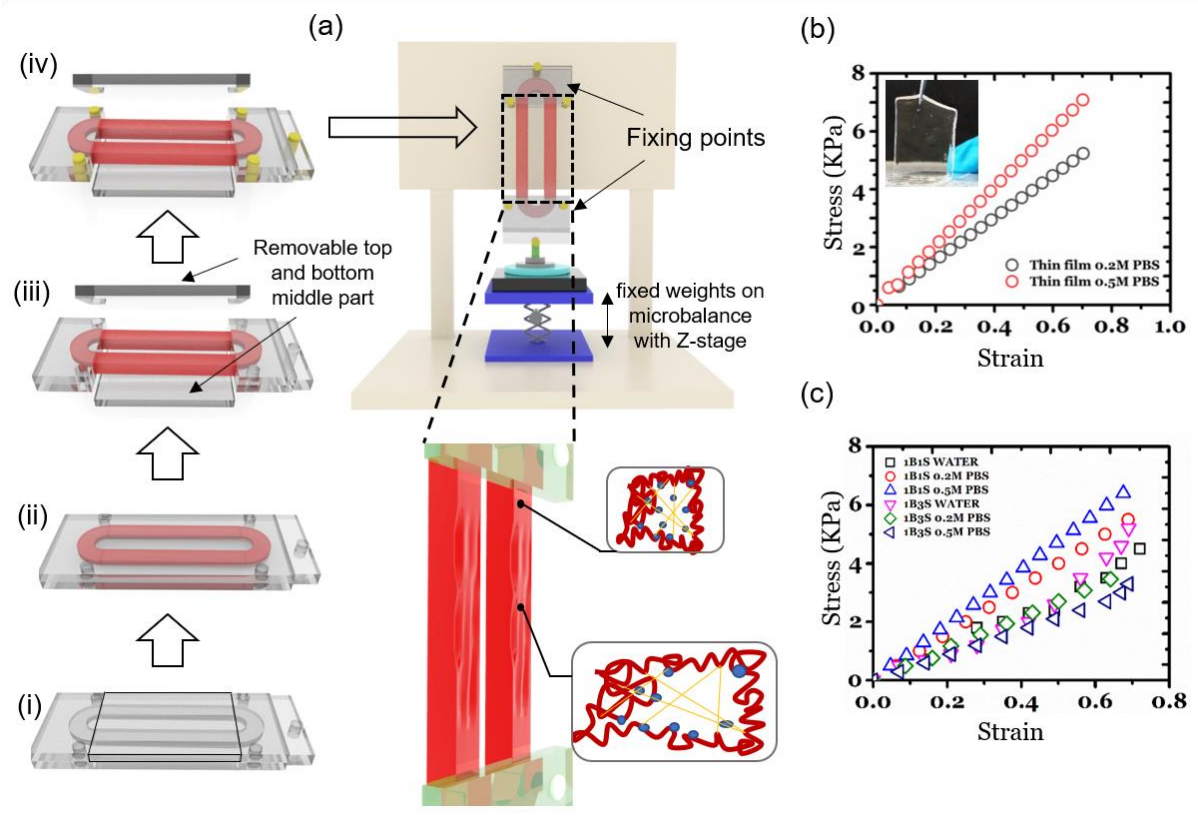


**Figure 3.** Mechanical property characterization (a) in-house developed clamp-free tensile tester for swelling hydrogels, with procedures (i) to (iv) showing the molding setup where as-fabricated PAAm composites can be directly integrated with the tensile tester; (b) & (c) strain-stress relationship of (b) the non-functional substrate PAAm thin film, immersed in 0.2M and 0.5M PBS solutions for 10 minutes; and (c) the functional PAAm-SA immersed in DI water, 0.2M and 0.5M PBS solutions for 10 minutes.

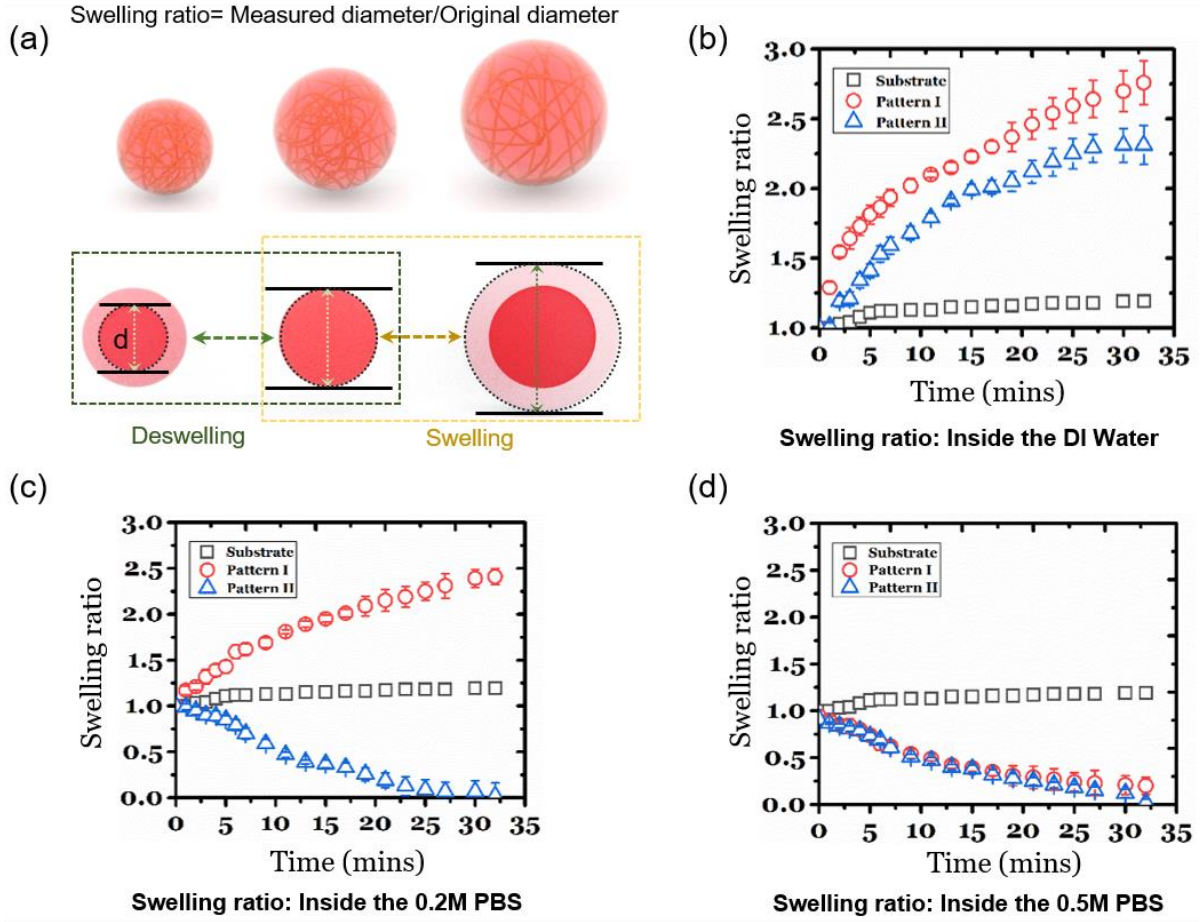


**Figure 4.** (a) Swelling ratio characterization using free standing hydrogel spheres; (b) – (d) Swelling ratio vs. Time – for non-functional substrate (PAAm), and Pattern I & II (PAAm-SA) samples immersed in (b) DI water; (c) 0.2M PBS; and (d) 0.5M PBS.

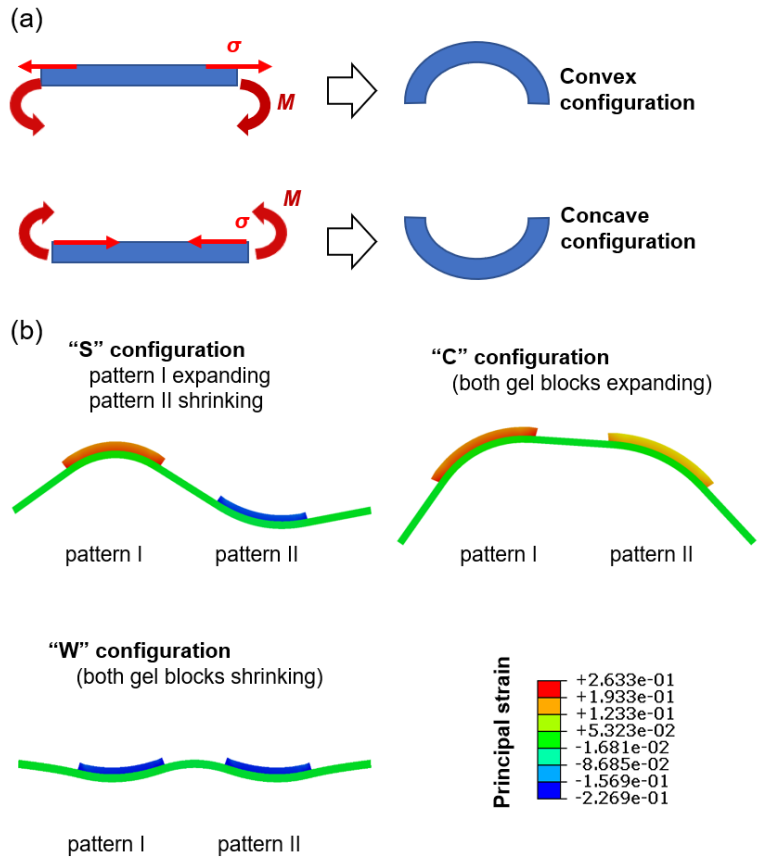


**Figure 5.** Mechanical model of the reconfigurable deformation: (a) convex and concave configuration due to bending moment; (b) numerical simulation results showing three different configurations induced by swelling and deswelling of Pattern I and II, based on the obtained mechanical property and swelling ratio results.

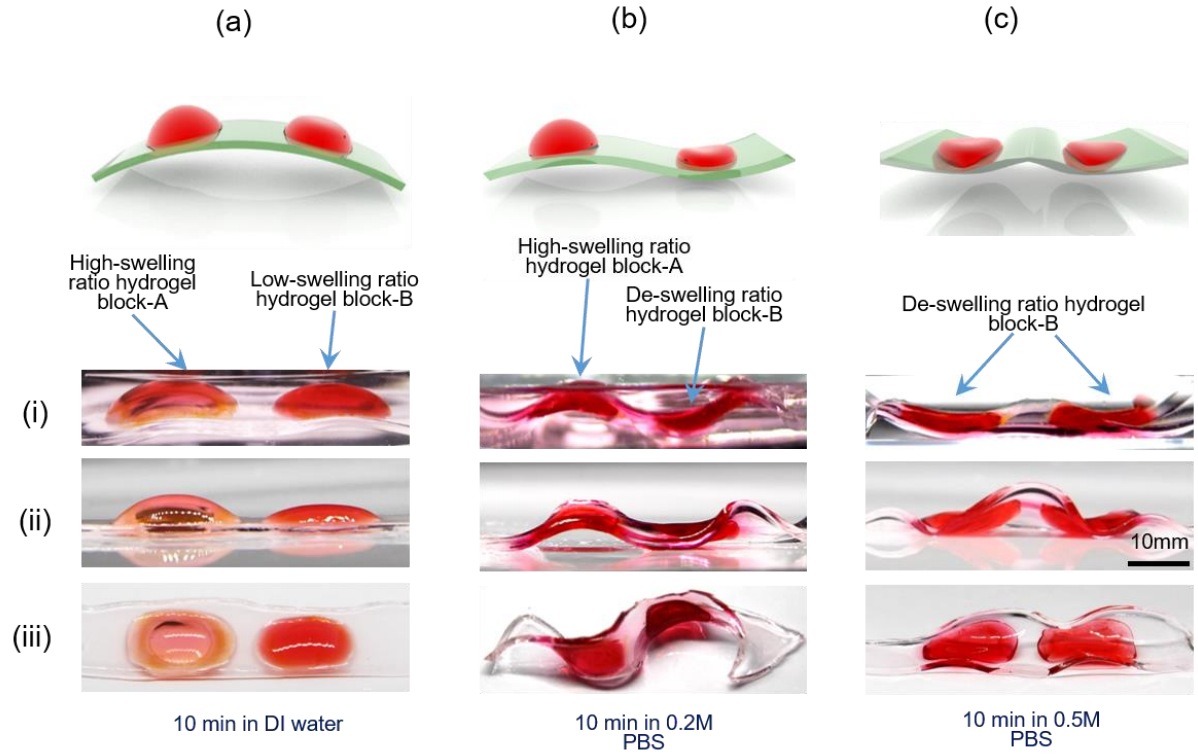

**Figure 6.** Representative complex 3d conformable configurations with mask-free swelling/deswelling, deformed from 2D patterned functional/non-functional hydrogels ionic imbalance. (a) Concave deformation achieved by immersing the transducers in DI water. (b) Buckling mismatch configuration of hydrogel transducer in 0.2M PBS, (c) Co-operative deswelling of both high and low sodium acrylate patterns in 0.5M PBS. Row (i) to (iii) represent different viewing angles and condition: (i) Structure in solution – side view; (ii) Structure in air (gravity in play) – side view; (iii) Structure in air – top view.

**ToC**

Reconfigurable soft structure 3D morphing has been enabled by the co-operation between swelling-mismatch of functional groups patterned as heterogeneous hydrogel bi-layers. Multiple deformation states can be driven by in-plane and through-thickness gradient during external stimulation such as ionic concentration change. The fabrication process is enabled by wetting-controlled surfaces empowered open-microfluidics in a "two-parallel plate" (Hele-Shaw Cell) system.

**Keyword**
Heterogeneous hydrogel, droplet microfluidics, responsive swelling, flexible sensors, layer by layer

Sreepathy Sridhar, Cong Wang, Jonathan G. Terry, Xue Chen, Ansu Sun, Zhenghong Li, Haibao Lv, Ben B. Xu and Yifan Li*

**Controlled Co-operative Wetting Enabled Heterogeneous Structured 3D Morphing Transducers**

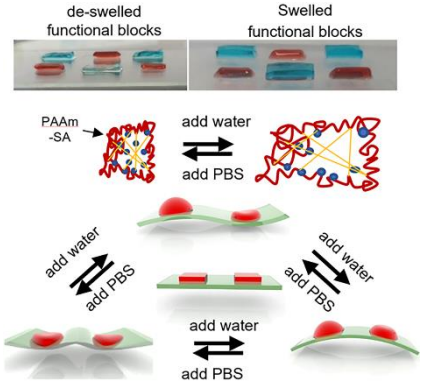

# Supporting Information

## Controlled Co-operative Wetting Enabled Heterogeneous Structured 3D Morphing Transducers

*Sreepathy Sridhar[1], Cong Wang[1], Jonathan G. Terry[2], Xue Chen[1], Ansu Sun[1], Zhenghong Li[3], Haibao Lv[3], Ben B. Xu[1] and Yifan Li[1] **

*Side-view observation of wetting process in TPP system:*

Due to the large aspect ratio (plate width : gap height) of the TPP system, typically larger than 100:1, the side-view observations (Fig. **1b** and **2c**) could be challenging if the DSA (Droplet Shape Analyzer) does not have a tilt-tip stage. We have therefore created an in-house developed system (**Fig. S1**).

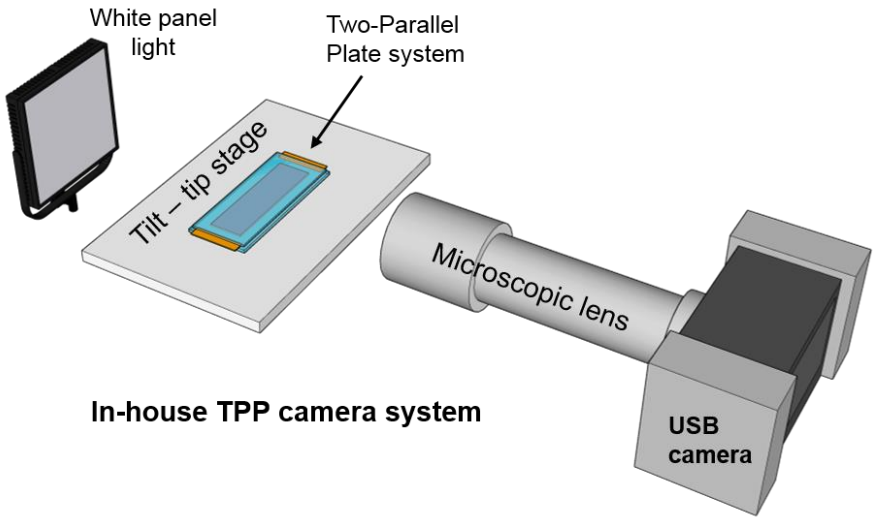


**Figure S1.** In-house developed camera system for side-view observation of the wetting process, through the gap of the TPP parallel plate system.

As the gap height $g$ is in the range of 0.025 – 3 mm, long working distance microscopic lenses were employed and put on a USB camera (Thorlabs DCC1645C). Another critical element is the tilt-tip stage. The high aspect ratio ( > 100:1) of the two-plate system means the tilting angle needs to achieve a minimum resolution of 0.5 ° ≈ arctan (0.01).

*Numerical Simulation Details:*

By immersing the gel structure in the PBS solution, the functional gel blocks will expand (swell) or shrink (de-swell) depending on the concentration of PBS solution. The mismatched strains between the expanded/contracted functional gel blocks and the non-functional substrate will induce an internal stress, which leads to the bending behaviour of the gel structure. To simultaneous simulate the expansion (swelling) and contraction (de-swelling) of different gel blocks under the same ionic environment (i.e. same PBS solution), complex diffusion kinetics must be developed, and the resulted coding and computation will be time-consuming. Therefore, we used the thermal expansion and contraction instead, which has already been incorporated in most commercial computing software. It is noted that our aim is to demonstrate a proof-of-concept simulation targeting at structure deformation design, not to precisely model the different diffusion processes.

The commercial finite element software ABAQUS is adopted to conduct the simulations. 2D plane-strain condition is assumed. Both the functional gel blocks and the non-functional substrate are modelled as hyper-elastic incompressible neo-Hookean material. For the functional gel, a non-zero thermal expansion coefficient is introduced. Moreover, the element type of "Coupled Temperature-Displacement" is selected and the step of "Coupled temp-displacement" is created to conduct the coupled thermo-mechanical analysis, i.e. solving simultaneously the mechanical equilibrium equation (for deformation) and the heat transfer equation (for temperature) with thermal expansion/contraction considered. The surface heat flux entering the gel is used as thermal load to induce the thermal expansion while the one leaving the gel is used for thermal contraction.

Three simulation results corresponding to three tests are shown in the paper: (1) one gel block expands with the principal strain around 0.25 and the other one contracts with the principal strain around −0.2, corresponding to the test of immersing the heterogeneous gel structure in the 0.2M PBS solution for 2 minutes; (2) both gel blocks contract with the principal strain around −0.2, corresponding to the test of immersing the gel structure in the 0.5M PBS solution for 2 minutes; (3) one gel block expands with the principal strain around 0.25 and the other one expands with the principal strain around 0.1, corresponding to the test of immersing the gel structure in the DI water for 2 minutes.

Besides 2D simulations, we have also performed a 3D simulation shown in **Figure S2** as an extra example of a structure incorporating more functional gel blocks, thus exhibiting more complex 3D wavy configuration.

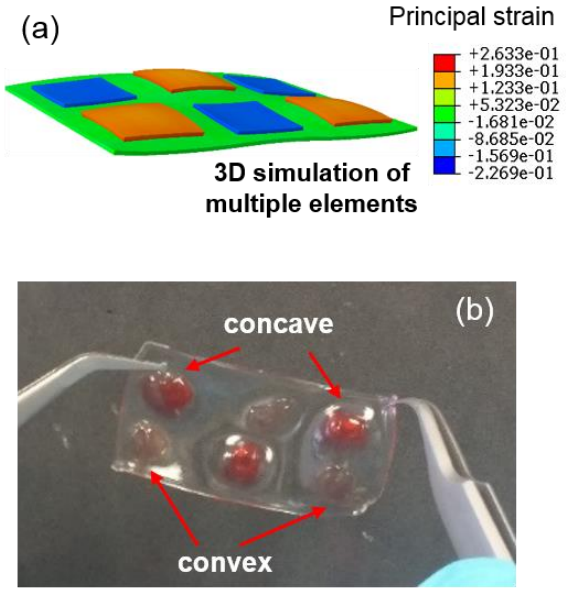


**Figure S2.** (a) 3D simulation of multiple elements; (b) Multiple concave and convex 3D wavy configuration obtained during experiment.